Upgrading CCIR's f_oF2 maps using available ionosondes and genetic algorithms

Erika Gularte[1], Daniel D. Carpintero[2], Juliana Jaen[1]

[1]Geodesia Espacial y Aeronomía, Facultad de Ciencias Astronómicas y Geofísicas, Universidad Nacional de La Plata, Argentina.

[2]Dinámica de Galaxias, Facultad de Ciencias Astronómicas y Geofísicas, Universidad Nacional de La Plata and Instituto de Astrofísica de La Plata, CONICET-UNLP, Argentina.

Abstract

We have developed a new approach towards a new database of the ionospheric parameter f_oF2. This parameter, being the frequency of the maximum of the ionospheric electronic density profile and its main modeller, is of great interest not only in atmospheric studies but also in the realm of radio propagation. The current databases, generated by CCIR (Committee Consultative for Ionospheric Radiowave propagation) and URSI (International Union of Radio Science), and used by the IRI (International Reference Ionosphere) model, are based on Fourier expansions and have been built in the 60s from the available ionosondes at that time. The main goal of this work is to upgrade the databases by using new available ionosonde data. To this end we used the IRI diurnal/spherical expansions to represent the f_oF2 variability, and computed its coefficients by means of a genetic algorithm (GA). In order to test the performance of the proposed methodology, we applied it to the South American region with data obtained by RAPEAS (Red Argentina para el Estudio de la Atmósfera Superior, i.e. Argentine Network for the Study of the Upper Atmosphere) during the years 1958 to 2009. The new GA coefficients provide a global better fit of the IRI model to the observed f_oF2 than the CCIR coefficients. Since the same formulae and the same number of coefficients were used, the overall integrity of IRI's typical ionospheric feature representation was preserved. The best improvements with respect to CCIR are obtained at low solar activities, at large (in absolute value) modip latitudes, and at night-time. The new method is flexible in the sense that can be applied either globally or regionally. It is also very easy to recompute the coefficients when new data is available. The computation of a third set of coefficients corresponding to days of medium solar activity in order to avoid the interpolation between low and high activities is suggested.The same procedure as for f_oF2 can be perfomed to obtain the ionospheric parameter *M(3000)F2* .

Keywords: f_oF2 maps, genetic algorithm, ionosphere, F region

1. Introduction

A more accurate prediction and forecast capability of the ionospheric climate and weather is an integral element of the current space weather activities worldwide (Cander, 2015), because the ionosphere plays a critical role for all techniques, either ground-based or space-based, that depend on radio wave signals travelling through it such as radio astronomy or Earth observation from space (Hargreaves, 1992).

The core model used for the ionospheric study is that of the International Reference Ionosphere (IRI). IRI is a data-based model of the ionosphere that describes the electron and ion densities and temperatures in the Earth's ionosphere at altitudes in the range from 50 km to 2000

km. Since its inception in 1969 the model has been steadily improved as new data became available, as old data sources were fully exploited and as new modeling techniques were applied (Bilitza,1990; Bilitza and Rawer, 1996; Bilitza et al., 2014; Bilitza, 2015). The IRI model is the standard model for the ionosphere recommended by both the Committee on Space Research (COSPAR) and the International Union of Radio Science (URSI), and also by the International Telecommunication Union (ITU) and the International Standardization Organization (ISO).

The IRI electron density profile is critically dependent on the correct values of the *F*2 layer peak height and density, *hmF*2 and *NmF*2 (or f_oF2). To compute these parameters, the IRI model applies a numerical mapping technique based on orthogonal Fourier functions (ITU, 2009). This model uses the CCIR (Committee Consultative for Ionospheric Radiowave propagation) numerical map model (Jones and Gallet, 1962; Jones et al., 1969; CCIR 1966). IRI recommends to use the CCIR numerical map coefficients over land areas and the URSI numerical map coefficients (Fox and McNamara, 1988; Rush et al.,1989) over the oceanic areas. The CCIR map is based on monthly median values obtained by the worldwide network of ionosondes (about 150 stations) during the years 1954 to 1958, altogether about 10,000 station-months of data. On the other hand, the URSI map is based on 45,000 station-months of ionosonde data and includes theoretical considerations to establish screen points in data-sparse areas of the world.

The frequency f_oF2 and the propagation factor *M(*3000*)F*2, closely related to *hmF*2, are routinely monitored by the worldwide network of ionosondes from the ground and a long data record going back to the late 1950s exists. However, the distribution of the ground-based ionosondes is too sparse to capture the large-scale features of the ionosphere. Therefore, in order to obtain more accurate and reliable ionospheric maps, different methodologies were developed.

To reconstruct maps of f_oF2, Liu et al. (2008) used the Kriging algorithm, which is a widely used interpolation method originally developed for geology (Krige, 1951; Matheron, 1963). The Kriging algorithm is more accurate when larger numbers of recorded data are utilized.

In the past decades the technique of neural networks (NNs) has been successfully employed by a number of researches for prediction of ionospheric parameters, such as f_oF2, *M(*3000*)F*2 and total electron content (TEC) (Scotto, 2001; Xenos, 2002; Habarulema et al., 2009; McKinnell and Oyeyemi, 2010), specially over particular regions. A neural network is a program trained to learn the relationship between the inputs and the outputs (Haykin, 1994; Fausett, 1994). After determining the relationship, the model can predict the values at any given time and location. Then, to avoid the local minimum phenomenon in most NNs applications, the GA-NNs models were developed (Wang et al., 2013; Huang et al. 2015), where a genetic algorithm (GA) is used to optimize the initial weights of the NNs. To obtain a good spatial description with these models, long training samples are required, which are prone to overfit and can lead to unexpected results with noisy data.

On the other hand, data assimilation techniques to describe ionospheric conditions far from an average quiet time behavior also were developed (Galkin et al., 2012 and references therein). In addition, Mandrikova et al. (2015) suggested a multiscale wavelets decomposition to determine the time variation of f_oF2 ; and Jiang et al. (2016) reconstructed the vertical electron density profile and estimated the parameters f_oF2 and *hmF*2 based on vertical TEC data by using the simulated annealing algorithm.

The aim of this paper is to upgrade the CCIR numerical map coefficients for f_oF2 by using both a genetic algorithm and new available observed data. That is, with the increased data base that

accumulated since the CCIR/URSI models were built, and by applying the modern technique of genetic algorithms, we expect that a better representation of f_oF2 (or *NmF*2) can be achieved, leading to an increase in accuracy of the ionospheric model. We describe the proposed methodology in Section 2. In Section 3 we present an application to the South American region. We analyze and illustrate the results in Section 4, followed by conclusive remarks in Section 5.

2. Methodology

We used the IRI numerical mapping technique (ITU, 2009) based on the CCIR model (Subsection 2.1) to compute the f_oF2 frequencies. The numerical map coefficients were computed to match the ionosondes measurements by means of a genetic algorithm (Subsection 2.2).

2.1. Diurnal/Spherical Expansions for f_oF2

Following a numerical mapping procedure developed by Jones and Gallet (1962), the diurnal variation of the f_oF2 for a given geographical location (latitude φ, longitude λ) and a given universal time (τ) is computed in the IRI model (ITU, 2009) by means of:

$$f_oF2\,(\varphi,\lambda,\tau) = A_0(\varphi,\lambda) + \sum_{i=1}^{6}(A_{2i-1}\,(\varphi,\lambda)\cos(i\tau) + A_{2i}\,(\varphi,\lambda)\sin(i\tau)), \quad (1)$$

that is, a Fourier series expansion, up to sixth order, amounting to a total of 13 coefficients.

Then, each Fourier coefficient, in turn, is computed by means of a spherical harmonics expansion in geographical coordinates, up to degree 8, which means there is a total of 76 coefficients:

$$A_i(\varphi,\lambda) = \sum_{j=0}^{J(0)} C_{ij0}\ P_{j0}(\varphi,\lambda) + \sum_{k=1}^{8}\sum_{j=0}^{J(k)}(C_{ij(2k-1)}\cos(k\lambda) + C_{ij(2k)}\sin(k\lambda))P_{jk}(\varphi,\lambda), \quad (2)$$

where $J(0)$ and $J(k)$ are the maximum order of the expansions of degree 0 and *k*, respectively, and

$$P_{jk}(\varphi,\lambda) = (\sin\chi\,(\varphi,\lambda))^j(\cos\,\varphi)^k \ \text{ and } \ \chi(\varphi,\lambda) = \tan^{-1}\left(\frac{I(\varphi,\lambda)}{\sqrt{\cos\lambda}}\right), \quad (3)$$

where $I(\varphi,\lambda)$ stands for the true magnetic dip angle at a height of 350 km over the considered location.

In short, one day of the global f_oF2 distribution requires 13 diurnal × 76 spherical = 988 coefficients C_{ijk}. The coefficients are computed twice: one set is computed for high solar activity and another one for low solar activity. For intermediate levels of solar activity, a linear interpolation is done. Taking into account that each month of the year has its own set of coefficients, and that two different levels of solar activity are considered, the total number of coefficients needed to compute f_oF2 at any location or time is therefore 23,712 (= 988 × 12 months × 2 levels of solar activity).

When a universal time τ and a location (φ,λ) are specified, the model uses τ to obtain the set of 988 coefficients C_{ijk} interpolated to the specific level of solar activity and day of the month, and then uses Eq. (2) to compute the 13 coefficients A_i of Eq. (1) to finally obtain the f_oF2 value.

2.2. Genetic algorithm optimization

A genetic algorithm (GA) (Goldberg, 1989; Davis, 1991) is an optimization algorithm that uses the concepts of natural selection and biological evolution to achieve its goal, i.e., to find the maximum of a given function. Its main advantages over other methods are (a) its ability to cope

with very complex functions, in particular with non-analytical functions of many variables, and (b) its ability to find the global maximum even when there are multiple local maxima, which is usually the case with functions of many variables. GAs has been successfully applied on other disciplines (Charbonneau, 1995; Gularte and Carpintero, 2006; Carpintero et al., 2013) to solve mixed problems.

Our implementation of a GA is based on the PIKAIA paradigm (Charbonneau and Knapp, 1995). Fig.1 shows, in a general case, the flow chart followed by our GA in order to find the maximum of a given function, called the *fitness*. The algorithm starts by disseminating *N* points at random all over the domain of the function. Each point is called an *individual*, or *phenotype*. This set of *N* individuals is the first *generation*. Next, the fitnesses of each individual are computed, that is, the function to be maximized is evaluated at the points corresponding to the individuals. A greater fitness indicate a greater possibility that the individual is near the global maximum.

Once the first population is set, the cycle of reproduction is initiated by translating the phenotype to a *genotype*. The translation consists in taking the digits of the independent variables of each individual and putting them one after another, thus forming a string of digits or *cromosome* corresponding to that individual. This step is merely a tool to facilitate the following operations. Next, two of the inhabitants are selected to be parents. This selection is done according to the fitness: higher fitnesses convey a higher probability of being chosen, this probability being controlled by a selection pressure parameter. Once the couple is selected, they breed by splitting their genotypes at a ramdonly chosen point of their cromosomes, the same point for both, and crossing the resulting chunks. Also, these fresh genotypes are subjected to mutation of one or more of its genes, that is, its digits. This mutation ensures that the domain is thorougly explored in search for different maxima, avoiding the algorithm to be trapped in a local one. After crossing and mutation, the resulting two siblings are decoded, that is, their strings of integers are translated back to a set of real numbers, thus becoming two new points in the domain of the function, or citizens of the population, the fitnesses of which now have to be computed. This is repeated *N*/2 times, after which a whole new generation has been created. This new generation will have, on average, better fitnesses than the previous one (Charbonneau and Knapp, 1995).

A reproduction plan should be used to choose how the new individuals are to be inserted into the population, and how the old ones should be deleted. In all our runs, a reproduction plan was used which choose the best *N* among the 2*N* individuals of both the old and the new generations. These chosen ones constitute the population of the second generation. This cycle is repeated until *M* generations have passed, although one may continue the algorithm from the last generation if desired. The fitness of the fittest individual of the last generation is the result: the point of the domain corresponding to a maximum value of the function, or, at least, a point very close to the one corresponding to that maximum.

In orden to adapt this algorithm to compute the coefficients defined in Section 2.1 the following considerations were made. Our unknowns are the 1,976 coefficients corresponding to a given month (i.e., 13 diurnal × 76 spherical × 2 levels of solar activity). Therefore, we have a fitness function of 1,976 variables. Each individual will be a point in the domain of these variables, that is, a complete set of coefficients. The genotype will be the string of the digits of the 1,976 coefficients. The fitness function f was defined as

$$f = \frac{1}{\sum_{i=1}^{n_{\text{obs}}} |f_{\text{o}}F2(\varphi,\lambda,\tau) - f_{\text{o}}F2_{\text{Obs}}|}, \tag{4}$$

where n_{obs} is the number of observations used for the month (from any time and location), $f_{\text{o}}F2(\varphi, \lambda, \tau)$ are the frequencies computed by Eq. (1) with the coefficientes of the individual, and $f_{\text{o}}F2_{\text{Obs}}$ are the observed frequencies. Note that f is a measure of how well the set of $f_{\text{o}}F2$ frequencies computed with a given set of coefficients (a point in the domain) fit the observed set of frequencies $f_{\text{o}}F2_{\text{Obs}}$. The fitness function has been chosen as simple as possible since its repeated evaluation during the GA process is computationally very demanding.

The initial population is generated by choosing, for each coefficient of each individual, a random value between +5% and –5% of the corresponding CCIR coefficient. These initial values were chosen in order to be not too far from the CCIR solution, which is itself a good solution. Also, as the domain increases, more difficult is for the algorithm to arrive at a solution, so the chosen interval of ±5% was found to be a good compromise.

The population size was set at 5100 individuals, a number chosen according to the memory capacity of our computers (recall that each phenotype represents a set of 1,976 coefficients). Also, a combined full generational replacement reproduction plan was considered: once a full fresh set of *N* individuals was generated, we sorted them by fitness with the *N* individuals of the generation that gave rise to them, and chose among the 2*N* resulting individuals the fittest *N* as the new generation. Finally, the number of generations through which the population is to be evolved was set in 500, which determines the end of the search. Instead of a number of generations, we may have chosen a given value of f in order to finalize the program, but we decided not to do that because the ideal maximum of f is infinite, and this makes difficult to foresee which maximum value of f will correspond to a good fit. Anyway, a given run may always be continued for more generations as needed, if the final fit were considered not good enough.

To achieve more efficiency in computing time, the program, written in standard FORTRAN77, was parallelized by using the MPI paradigm. The parallelization region corresponds to the computation of the fitness, which can be done for each individual independently from the others. This allows a near maximum gain in computation time, given that the fitness is by far the most demanding part of the algorithm.

The entire process (i.e., 500 generations) was run 12 times, each one corresponding to a different month of the year. In the end, we obtained the 23,712 coefficients (= 1,976 × 12 months) needed to compute the $f_{\text{o}}F2$ frequency for any desired time and location, that is, the global map of $f_{\text{o}}F2$.

3. Application/Datasets

In order to test the performance of the proposed methodology, we chose the South American region. Since the Argentine Network for the Study of the Upper Atmosphere (RAPEAS, for the Spanish acronym) compiled Argentine ionosondes data from 1958 on, a wealth of new data is available in the South American region. RAPEAS provides hourly $f_{\text{o}}F2$ measurements (most of them manually scaled) from seven ionosonde stations: Jicamarca, San Juan, Buenos Aires, Concepción, Trelew, Ushuaia and San Martín. The geographic coordinates and modip latitudes of each station are tabulated in Table 1 and their spatial distribution map is shown in Fig. 2. Note that this set of ionosonde stations cover a wide range of latitudes, from the equatorial up to the sub-auroral regions.

The dataset used for this work consists of 78,339 observed values of $f_{\text{o}}F2$ taken hourly and in quiet days from 1958 to 2009, covering many solar cycles.

We also obtained an additional set of about 100 observations from the ionosonde at La Plata. ($\varphi = -34.9,\ \lambda = 302.1$), corresponding to February, May, October and December 2012. Though the comparison of our model is to be done through the residuals and against the CCIR maps, we nevertheless set aside this data to compare predictions of both models.

4. Results and discussion

Once the coefficients were computed with the GA, we feeded them to the algorithm described in Subsection 2.1 in order to compute a new set of f_oF2 values, f_oF2_{GA} , at the times and places of all the observed points. These values were to be compared with the corresponding f_oF2 values obtained with the IRI algorithm using the CCIR maps, f_oF2_{CCIR}. In order to make this comparison, we first plotted both sets of f_oF2 values against the observed ones, f_oF2_{Obs} (Fig. 3). By fitting a straight line by least squares to both sets we obtained the equations shown at the top of the Figure. We see that, for the f_oF2_{GA} values, the slope is closer to 1 and the ordinate at the origin is closer to 0 than for those obtained with the CCIR ones. That is, in a mean sense, the GA coefficients produce a set of f_oF2 values closer to the observed ones.

To further quantify this difference, we computed the correlation coefficients (e.g., Press et al. 1992, Sec. 14.5) between the f_oF2_{GA} ($:= f_oF2^{\mathrm{GA}}$) and the f_oF2_{Obs} ($:= f_oF2^{\mathrm{Obs}}$) values, $\rho_{[\mathrm{GA\ Obs}]}$, and between the f_oF2_{CCIR} ($:= f_oF2^{\mathrm{CCIR}}$) and the f_oF2_{Obs} values, $\rho_{[\mathrm{CCIR\ Obs}]}$, by means of

$$\rho_{[\mathrm{GA\ Obs}]} = \frac{\sigma_{[\mathrm{GA}][\mathrm{Obs}]}}{\sigma_{\mathrm{GA}}\,\sigma_{\mathrm{Obs}}} := \frac{\sum_{i=1}^{n}\left(f_oF2_i^{\mathrm{GA}}-\mu_{\mathrm{GA}}\right)\left(f_oF2_i^{\mathrm{Obs}}-\mu_{\mathrm{Obs}}\right)}{\sqrt{\sum_{i=1}^{n}\left(f_oF2_i^{\mathrm{GA}}-\mu_{\mathrm{GA}}\right)^2}\sqrt{\sum_{i=1}^{n}\left(f_oF2_i^{\mathrm{Obs}}-\mu_{\mathrm{Obs}}\right)^2}} \tag{5}$$

and

$$\rho_{[\mathrm{CCIR\ Obs}]} = \frac{\sigma_{[CCIR][\mathrm{Obs}]}}{\sigma_{\mathrm{CCIR}}\,\sigma_{\mathrm{Obs}}} := \frac{\sum_{i=1}^{n}\left(f_oF2_i^{\mathrm{CCIR}}-\mu_{\mathrm{CCIR}}\right)\left(f_oF2_i^{\mathrm{Obs}}-\mu_{\mathrm{Obs}}\right)}{\sqrt{\sum_{i=1}^{n}\left(f_oF2_i^{\mathrm{CCIR}}-\mu_{\mathrm{CCIR}}\right)^2}\sqrt{\sum_{i=1}^{n}\left(f_oF2_i^{\mathrm{Obs}}-\mu_{\mathrm{Obs}}\right)^2}}, \tag{6}$$

where σ_X is the dispersion and μ_X the mean of the f_oF2_{i} values corresponding to set *X*, $\sigma_{[\,][\,]}$ are the covariances and n the number of observed points. The resulting values were $\rho_{[\mathrm{GA\ Obs}]} = 0.897$ and $\rho_{[\mathrm{CCIR\ Obs}]} = 0.869$. Though the two values are close to each other, the GA result is slightly better than the CCIR one. We made sure that the correlation coefficients were statistically significant by performing a Student *t* test on them (e.g., Press et al. 1992, Sec. 14.5), with $n - 2 = 78{,}337$ degrees of freedom. In both cases, the tests gave statistical significance at any prefixed level, that is, the area at the left of the observed *t* below the curve of the distribution of *t* gave unity. So, both sets of coefficients give f_oF2 values which are quite representative of the observed frequencies.

Due to the similarity of the correlation coefficients, we may ask whether the two sets are indeed statistically the same. To answer this, we computed the dispersions corresponding to both sets, and performed a Fisher *F* test on their quotient (e.g., Press et al. 1992, Sec. 14.2), with a null hypothesis that the samples belong to the same mother population. The resulting dispersions were $\sigma^2_{[\mathrm{GA\ Obs}]} = 0.043$ and $\sigma^2_{[\mathrm{CCIR\ Obs}]} = 0.061$, which, with $n - 1 = 78{,}338$ degrees of freedom for both samples, gave an observed *F* = 1.42. The *P*-value, that is, the area below the *F* distribution's curve at the right of the observed *F*, is 1. This means that the two samples are indeed statistically different at any level of significance.

Fig. 4 shows a histogram of the distribution of the relative errors $\Delta\varepsilon_{\mathrm{GA}} = (f_oF2_{\mathrm{GA}} - f_oF2_{\mathrm{Obs}})/f_oF2_{\mathrm{Obs}}$ (black bars) and $\Delta\varepsilon_{\mathrm{CCIR}} = (f_oF2_{\mathrm{CCIR}} - f_oF2_{\mathrm{Obs}})/f_oF2_{\mathrm{Obs}}$ (white bars). As

expected from our previous results, the resulting errors of the GA set are smaller in mean that those of the CCIR set. Besides, one can observe a systematic tendency of the latter in overestimating the frequency f_oF2 more than the former. At the same time, a trend towards more underestimation is visible in the GA set, though it is smaller than the above mentioned overestimation. It is worth noticing that more than 60% of the computed frequencies using the GA algorithm have relative errors between $-0.1 < \Delta\varepsilon_{\mathrm{GA}} < 0.1$, whereas less than 50% of the frequencies computed with the CCIR lie between those values.

Now, we want to analyze how these results depend on various variables that enter the computation of the f_oF2 frequency. We first divided our collection of observations in three sets, one corresponding to values of solar index *IG*12 > 120 (i.e., high solar activity), the second one to values of 40 < *IG*12 < 120 (medium solar activity), and the third to *IG*12 < 40 (low solar activity). We performed, for each of the three sets, the same computations and tests already described for the general case (i.e., slopes and ordinates at the origin of the least squares straight lines, correlation coefficients and their statistical signification, and dispersions for GA and CCIR with their *F* values and *F*-tests). Fig. 5 shows the corresponding plots of f_oF2_{GA} vs. f_oF2_{Obs} and f_oF2_{CCIR} vs. f_oF2_{Obs} for each interval of solar activity, together with the corresponding least squares fits. Table 2 shows the values of the rest of the indicators. Except for the medium solar activity, the conclusions are the same as in the general case: similar correlation coefficients, with that of the GA slightly better than that of the CCIR; both coefficients statistically significant (not shown in the Table); dispersion of the f_oF2_{GA} values less than that of the f_oF2_{CCIR} ones, and an *F* value which proves that the dispersions belong to different populations, that is, the *P*-value of the observed *F* is 1. For the medium solar activity, the conclusions are the same except for (a) the dispersions, which are inverted in magnitude, i.e., the one corresponding to the GA is slightly greater than that of the CCIR, and (b) the correlation coefficients are smaller than the other cases, that is, the fit to the observed values is poorer. It is worth noticing that both GA and CCIR correlation coefficients are worse than those of the general case. This may be probably due to the fact that the CCIR coefficients were computed separately in two subsets: one set is based on high solar activity days, and the other one based only on low solar activity days (see Subsection 2.1). Since an f_oF2 value is obtained by interpolating to the solar activity of the time of the computation, a medium solar activity is the less accurate situation. On the other hand, the GA coefficients, as already said, are always between 95% and 105% of the CCIR ones, and the computation of the f_oF2 values follows the same procedure as in the IRI algorithm. Thus, we expect a less accurate result at medium solar activities also in this case.

We also examined the behavior of the f_oF2 values in different seasons. Table 2 shows the statistical values. The conclusions are the same as in the general case. We note that the smaller dispersions are achieved in Summer.

We also studied how the f_oF2 values vary with modip latitude. The polar latitude is excluded due to the lack of observations. Table 2 resumes the obtained statistical values. Although the general result is similar to the other cases, we want to emphasize two points. First, at the middle and high latitudes the fits, both for the GA and the CCIR models, are noticeably better than in the general case, whereas in the equatorial region the opposite is true. This last result may be due to the fact that the IRI mathematical model is less accurate in the equatorial band (McKinnell and Oyeyemi , 2010). Second, in the subauroral zone the f_oF2_{GA} values give a considerable better result than the f_oF2_{CCIR} values.

Finally, we studied the daily variations of the f_oF2 comparisons. To this end, we took the f_oF2 values corresponding to a interval near the noon and another one near the midnight. Table 2 shows the results. We note that the night-time values are similar to the general ones, but at noon the correlation is slightly worse, both for the GA and the CCIR models.

We show now some examples of the behavior of the GA-computed values of f_oF2 . We first computed for each observed day the quantity

$$\Delta f_c = \sum_{i=0}^{23} |f_oF2_{\text{GA}} - f_oF2_{\text{Obs}}| \ , \tag{7}$$

where the sum is over all the hours of the corresponding day. After this, we sorted all the resulting Δf_c according to their values, from the best result (the smallest number) to the worst one (the biggest number). From this list, we chose, among the best days, that with 24 observed hours; the same we did among the worst days. Fig. 6 shows the observed, GA-computed and CCIR-computed f_oF2 values of these best and worst days. For the best day (Fig. 6, left), we see that the CCIR prediction is very good indeed, but the GA prediction is even better. For the worst day (Fig. 6, right) we see that neither the CCIR nor the GA can reproduce well the observations, though the GA prediction performs slightly better. Note that the observations correspond to the Jicamarca station, near the Equator, which is therefore in a region where the mathematical model may be not good enough.

Next, in order to compare more directly the GA-based values of f_oF2 with those obtained with the CCIR coefficients, we computed for each observed day the quantity

$$\Delta f_{cp} = \sum_{i=0}^{23} \left(|f_oF2_{\text{GA}} - f_oF2_{\text{Obs}}| - |f_oF2_{\text{CCIR}} - f_oF2_{\text{Obs}}|\right) , \tag{8}$$

with the sum again over all the observed hours of the corresponding day. As before, we chose a best and a worst day. The best one (Fig.7, left) shows that while both the CCIR and the GA results follow the general pattern of the observed values, the GA values fit them far better. For the worst day (Fig.7, right), we have an example of the CCIR result outperforming that of the GA on most hours of the day, though, again, both follow the general trend of the observed pattern.

In order to show an example of the regional behaviour of the results, we show in the left panels of Figs. 8 and 9 contour maps of f_oF2_{GA} for the South American continent, both in the daytime (16:00 local time for the central stripe of the map, Fig. 8) and at night-time (23:00 local time, Fig. 9). Figs. 8 and 9 also show the corresponding differences $f_oF2_{\text{GA}} - f_oF2_{\text{CCIR}}$ (right panels).

Finally, we compared the predictions of both models for a set of about 100 data taken with the ionosonde at La Plata, Argentina, not included in the set of observations used to compute the GA coefficients. These data correspond to 12:00 local time for different days and months of 2012. Fig. 10 shows the outcome for the entire set. From left to right, the four groups shown in the Figure correspond to February, May, August and October, respectively. The mean value of $|\Delta\varepsilon_{\text{GA}}|$ is 0.092, and the mean value of $|\Delta\varepsilon_{\text{CCIR}}|$ is 0.153, showing once again the slight improvement of the GA algorithm over the CCIR map.

5. Conclusion

A methodology to upgrade f_oF2 maps over a given region by means of a genetic algorithm optimization was presented. For the f_oF2 ionospheric parameter, the IRI numerical mapping technique based on an orthogonal Fourier decomposition was applied, but a new set of coefficients (23,712 in all) was obtained in order to improve the performance.

The new coefficients were computed by the optimization of a merit function of the differences between the f_0F2 values obtained with those coefficients and the observed datasets obtained from seven ionosondes stations all around the South American region, which took hourly measurements for quiet days during the years 1958 to 2009, and covering a wide modip latitude and solar activity range.

These new coefficients provide a better global fit to the observed f_0F2 than the CCIR coefficients. This was quantified by computing the correlation coefficients between the observed and the computed values, both for the GA-based coefficients and the CCIR-based ones. The resulting values ($\rho_{[\mathrm{GA\ Obs}]} = 0.897$ and $\rho_{[\mathrm{CCIR\ Obs}]} = 0.869$) show that our new method performs indeed slightly better. We also confirmed that these two values correspond to statistically different results, that is, they represent two truly distinct performances. In this respect, it is worth to note that more than 60% of the computed frequencies using the GA algorithm have relative errors between $-0.1 < \Delta\varepsilon_{\mathrm{GA}} < 0.1$. Also, the variance of the relative difference between the computed values and the observed ones is less when the f_0F2 are computed with the GA coefficients ($\sigma^2_{[\mathrm{GA\ Obs}]} = 0.043$) than when they are computed with the CCIR coefficients ($\sigma^2_{[\mathrm{CCIR\ Obs}]} = 0.061$), that is, there is a smaller dispersion of relative errors with our coefficients.

Comparing against the observed values, the worst fits correspond to similar GA and CCIR values. In general, the trends showed by the CCIR results with solar index *IG*12 , modip latitude or hour of the day are the same as with our GA results. The best improvements with respect to CCIR are obtained at low solar activities, at large (in absolute value) modip latitudes, and at night-time.

Therefore, the new method allows to improve the coefficients of the IRI analytical model of f_0F2; it is flexible in the sense that a particular set of coefficients may be obtained not only regionally but also globally or locally, by simply using global or local available data. It is also very easy to recompute the coefficients when new data is available, for example when new stations are set or when additional observations are made along the time.

We plan to improve this methodology in several ways. For example, the computation of a third set of coefficients corresponding to days of medium solar activity is probably worth the effort, in order to avoid the interpolation between low and high activities. This can easily be done by simply augmenting the set of corresponding unknowns. Also, the same procedure as for f_0F2 can be perfomed to obtain the ionospheric parameter *M(*3000*)F*2, which allows to obtain the *hmF*2 parameter.

5.1. Acknowledgments

We thank two anonymous reviewers who helped to improve an early draft of this work. We wish to thank the following members of the RAPEAS network (Red Argentina para el Estudio de la Atmósfera Superior), which belongs to CONICET (Consejo Nacional de Investigaciones Científicas y Tecnológicas), that provided us with ionosondes data and their manual scaling: DIIV (Dirección de Investigaciones de la Armada), IAA (Instituto Antártico Argentino), ICATE (Instituto de Ciencias Astronómicas, de la Tierra y del Espacio) and Facultad de Ciencias Astronómicas y Geofísicas de la Universidad Nacional de La Plata. DDC wish to acknowledge grants from Conicet, Argentina (PIP 0436) and from the Universidad Nacional de La Plata, Argentina (Proyecto G127).

References

Bilitza, D., International Reference Ionosphere 1990, 155 pages, National Space Science Data Center, NSSDC/WDC-A-R&S 90-22, Greenbelt, Maryland, November 1990.

Bilitza, D. and Rawer K., International Reference Ionosphere, pp735-772, in: The Upper Atmosphere - Data Analysis and Interpretation, W. Dieminger, G. Hartmann and R. Leitinger (eds.), Springer-Verlag Berlin Heidelberg, 1996.

Bilitza D., D. Altadill, Y. Zhang, C. Mertens, V. Truhlik, P. Richards, L.-A. McKinnell, and B. Reinisch: The International Reference Ionosphere 2012 – a model of international collaboration. J. Space Weather Space Clim., 4(A07), pp. 1-12, doi:10.1051/swsc/2014004, 2014.

Bilitza D., The International Reference Ionosphere – Status 2013, Adv. Space Res., 55(8), 1914-1927, doi: 10.1016/j.asr.2014.07.032, 2015.

Cander, L.R., Forecasting foF2 and MUF(3000)F2 ionospheric characteristics - A challenging space weather frontier, Advances in Space Research 56(9), pp. 1973-1981, 2015.

Carpintero D.D., M.D. Melita and O.I. Miloni, DISTRA: A code to find invisible exoplanets, RevMexAA (SC), 43, pp. 68-70, 2013.

CCIR, Comité Consultatif International des Radiocommunications, Report 340-1, 340-6, ISBN 92-61-04417-4, Genève, Switzerland, 1966.

Charbonneau P., Genetic Algorithms in Astronomy and Astrophysics, Astrophysical Journal Supplement Series, 101, pp. 309-334, 1995.

Charbonneau P. and Knapp B., A User's Guide to PIKAIA 1.0, NCAR Technical Note 418+IA, National Center for Atmospheric Research, Boulder, Colorado, pp. 1-109, 1995.

Davis L., Handbook of Genetic Algorithms, Van Nostrand Reinhold, New York, pp. 1-101, 1991.

Fausett, L., Fundamentals of Neural Networks: Architectures, Algorithms, and Applications. Prentice-Hall, Upper Saddle River, New York, 1994.

Fox M.W.and McNamara L.F, Improved World-wide Maps of Monthly Median foF2, Journal of Atmospheric and Solar-Terrestrial Physics, 50(12) pp. 1077-1086, 1988.

Galkin, I. A., B.W. Reinisch, X. Huang and D. Bilitza, Assimilation of GIRO data into a real-time IRI, Radio Science, 47(4), pp. 1-10, doi: 10.1029/2011RS004952, 2012.

Goldberg D.E., Genetic Algorithms in Search, Optimization, & Machine Learning, Addison-Wesley, Reading, MA, 1989.

Gularte E. and Carpintero D.D., Sistemas estelares en equilibrio con algoritmos genéticos, Boletín de la Asociación Argentina de Astronomía, 49, pp.116-119, 2006.

Habarulema, J. B., L. A McKinnell,., P. J Cilliers and B. D.Opperman, Application of neural networks to South African GPS TEC modeling, Advances in Space Research, 43(11), 1711-1720, 2009.

Hargreaves, J.K.,The solar-terrestrial environment. Cambridge University Press, Cambridge, 1992.

Haykin S.; Neural networks: A comprehensive foundation. IEEE Computer Society Press and Macmillan, New York, 1994.

Huang Z., Q.B. Li and H. Yuan, Forecasting of ionospheric vertical TEC 1-h ahead using a genetic algorithm and neural network, Advances in Space Research, 55, pp. 1775-1783, 2015.

International Telecommunication Union (ITU), ITU-R reference ionospheric characteristics , Recomm. P1239-2(10/2009), Geneva, Switzerland, https://www.itu.int/rec/R-REC-P.1239/en, 2009.

Jiang C., G. Yang, P. Zhu, M. Nishioka, T. Yokoyama, C. Zhou, H. Song, T. Lan, Z. Zhao and Y. Zhang, Reconstruction of the vertical electron density profile based on vertical TEC using the simulated annealing algorithm, Advances in Space Research 57(10), pp. 2167-2176, 2016.

Jones W.B. and Gallet R.M., Representation of Diurnal and Geographical Variations of Ionospheric Data by Numerical Methods, Telecommunication Journal, 29, pp. 129-149, 1962.

Jones W.B, R.P. Graham, and M. Leftin [1969], Advances in Ionospheric Mapping by Numerical Methods, ESSA Technical Report ERL 107-ITS 75, US Government Printing Office, Washington DC, USA, 1969.

Krige D.G., A statistical approach to some basic mine valuation problems on the Witwatersrand, Journal of the Southern African Institute of Mining and Metallurgy, 52(11), pp. 264 - 266, 1951.

Liu R., G. Liu, J. Wu, B. Zhang, J. Huang, H. Hu and Z. Xu, Ionospheric foF2 Reconstruction and its Application to the Short-Term Forecasting in China Region, Chinese J. Geophys., 51, pp. 206–213,. doi:10.1002/cjg2.1212, 2008.

Mandrikova, O.V., N. V. Fetisova, R. T. Al-Kasasbeh, D. M. Klionskiy, V. V. Geppener and M. Y. Ilyash, Ionospheric parameter modelling and anomaly discovery by combining the wavelet transform with autoregressive models, Annals of Geophysics 58(5), p.A0550, 2015.

McKinnell, L. A., and. Oyeyemi E.O., Equatorial predictions from a new neural network based global foF2 model, Advances in Space Research, 46.8, pp. 1016-1023, 2010.

Matheron G., Principles of geostatistics, Economic Geology,. 58, pp. 1246–1266, doi: 10.2113/gsecongeo.58.8.1246, 1963.

Press W.H, S.A: Teukolsky, W.T. Vetterling, B.P. Flannery, Numerical recipes, Press Syndicate of the University of Cambridge, Cambridge, 1992.

Rush C., M. Fox, D. Bilitza, K. Davies, L. McNamara, F. Stewart, and M. PoKempner, Ionospheric Mapping – An Update of foF2 Coefficients, Telecommunication Journal, 56, pp. 179-182, 1989.

Scotto C., A study of real time ionospheric mapping by neural network, Physics and Chemistry of the Earth Part C Solar Terrestrial & Planetary Science, 26(5), pp.363-366, doi: 10.1016/S1464-1917(01)00014-9, 2001.

Wang R., C. Zhou C., Z. Deng, B. Ni and Z. Zhao, Predicting foF2 in the China region using the neural networks improved by the genetic algorithm, Journal of Atmospheric and Solar-Terrestrial Physics, 92, pp. 7-17, 2013

Xenos T.D., Neural-network-based prediction techniques for single station modeling and regional mapping of the foF2 and M (3000) F2 ionospheric characteristics, Nonlinear Processes in Geophysics, 9, pp. 477-486, 2002.

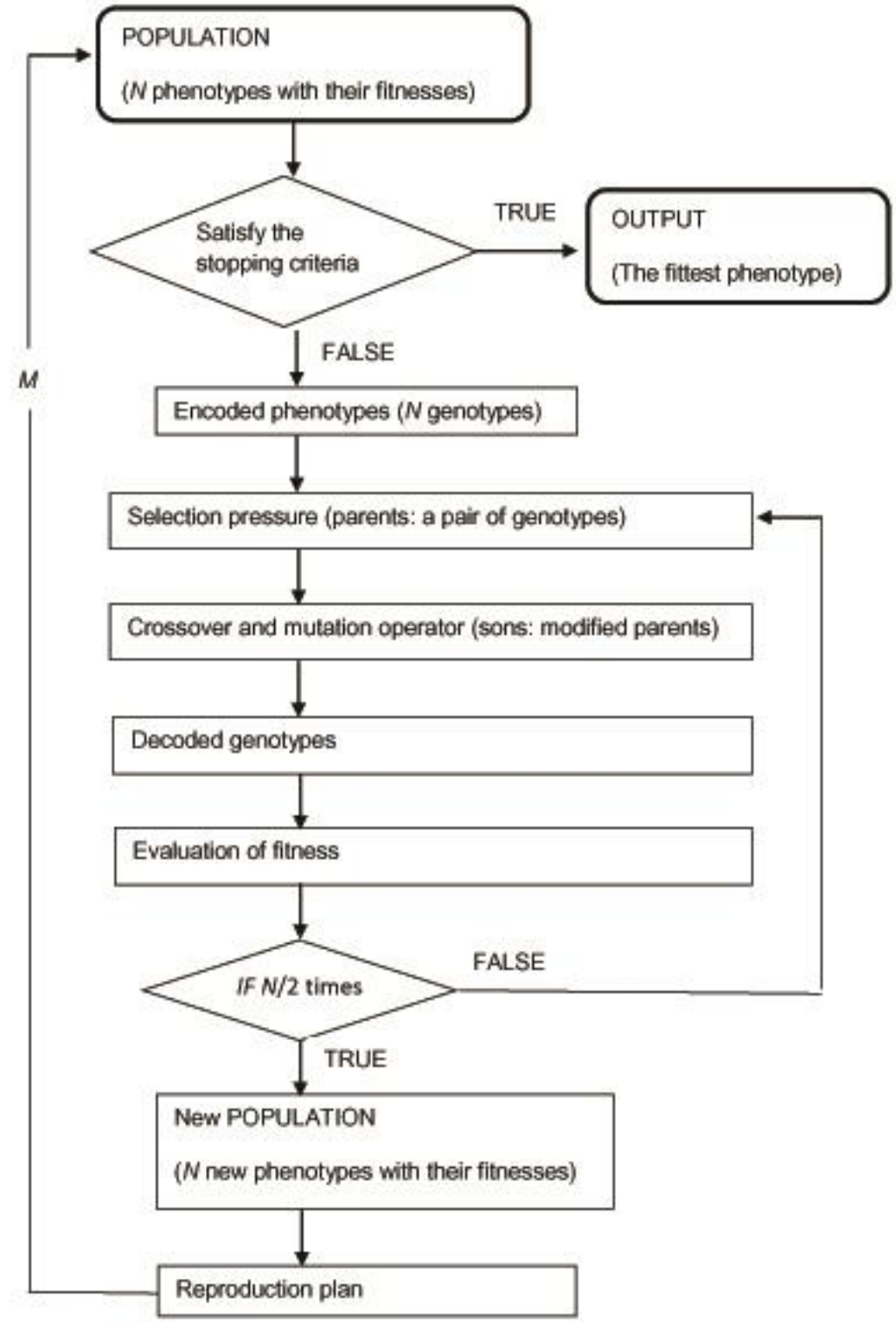

Figure 1. The flow chart followed by our GA in order to find the maximum of a given function, called the *fitness. N* is the number of individuals (phenotypes) in the population and *M* is the number of generations.

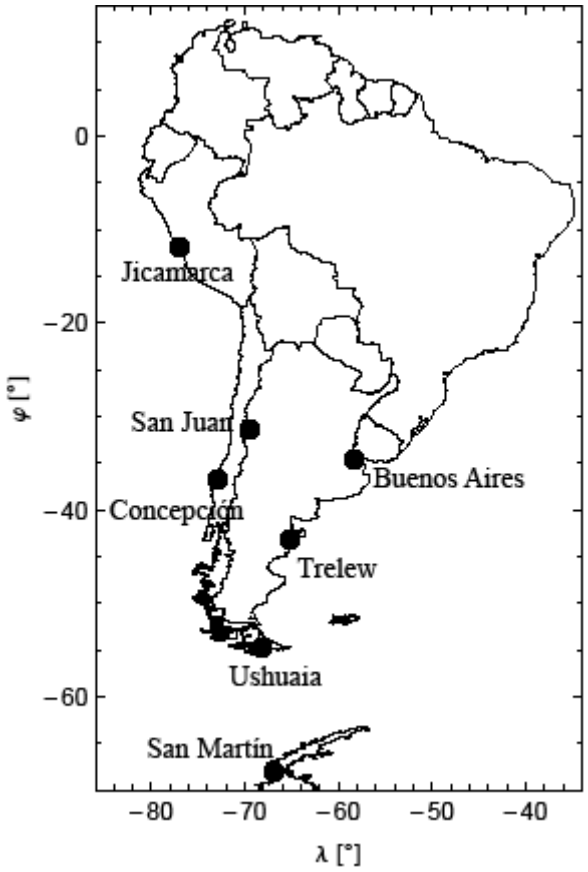

Figure 2. Distribution map of the ionosondes used in this study. Each ionosonde is marked with a big black point.

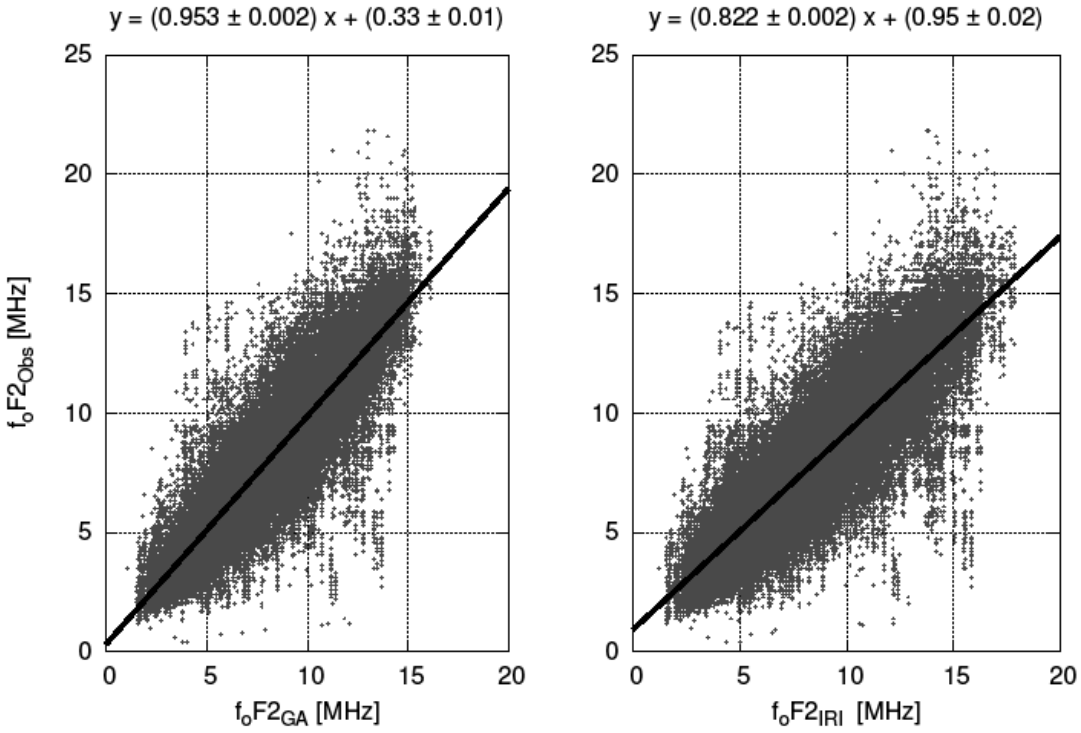

Figure 3. f_oF2 modeled values against the observed ones, f_oF2_{Obs}. Here f_oF2_{GA} are the f_oF2 values obtained with the GA coefficients and f_oF2_{CCIR} are the f_oF2 values using the CCIR maps. By fitting a straight line by least squares to both sets we obtained the equations shown at the top.

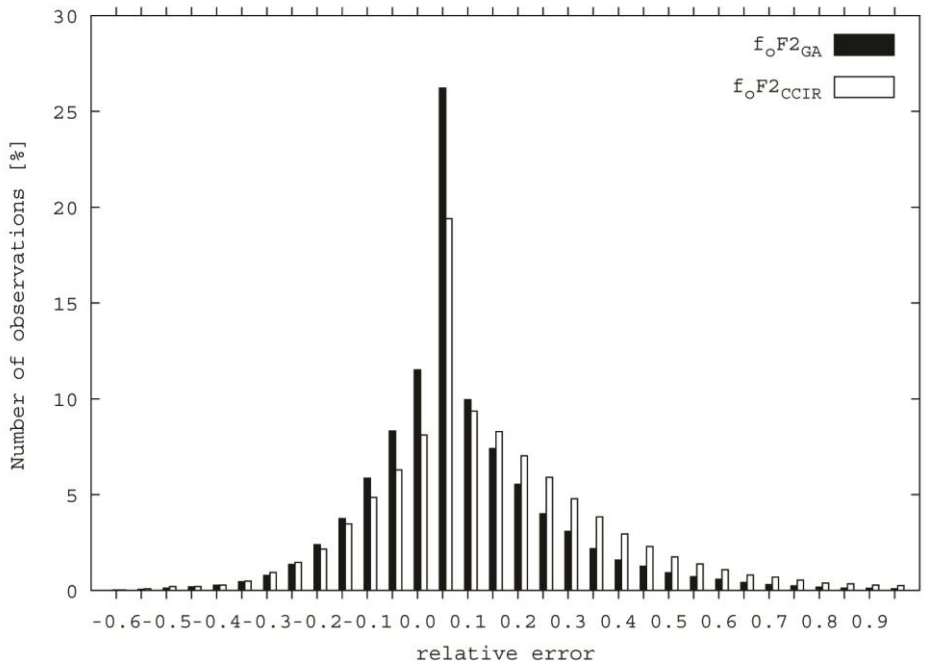

Figure 4. Histogram of the distribution of the relative errors $\Delta\varepsilon_{\mathrm{GA}} = (f_{\mathrm{o}}F2_{\mathrm{GA}} - f_{\mathrm{o}}F2_{\mathrm{Obs}})/f_{\mathrm{o}}F2_{\mathrm{Obs}}$ (black bars) and $\Delta\varepsilon_{\mathrm{CCIR}} = (f_{\mathrm{o}}F2_{\mathrm{CCIR}} - f_{\mathrm{o}}F2_{\mathrm{Obs}})/f_{\mathrm{o}}F2_{\mathrm{Obs}}$ (white bars).

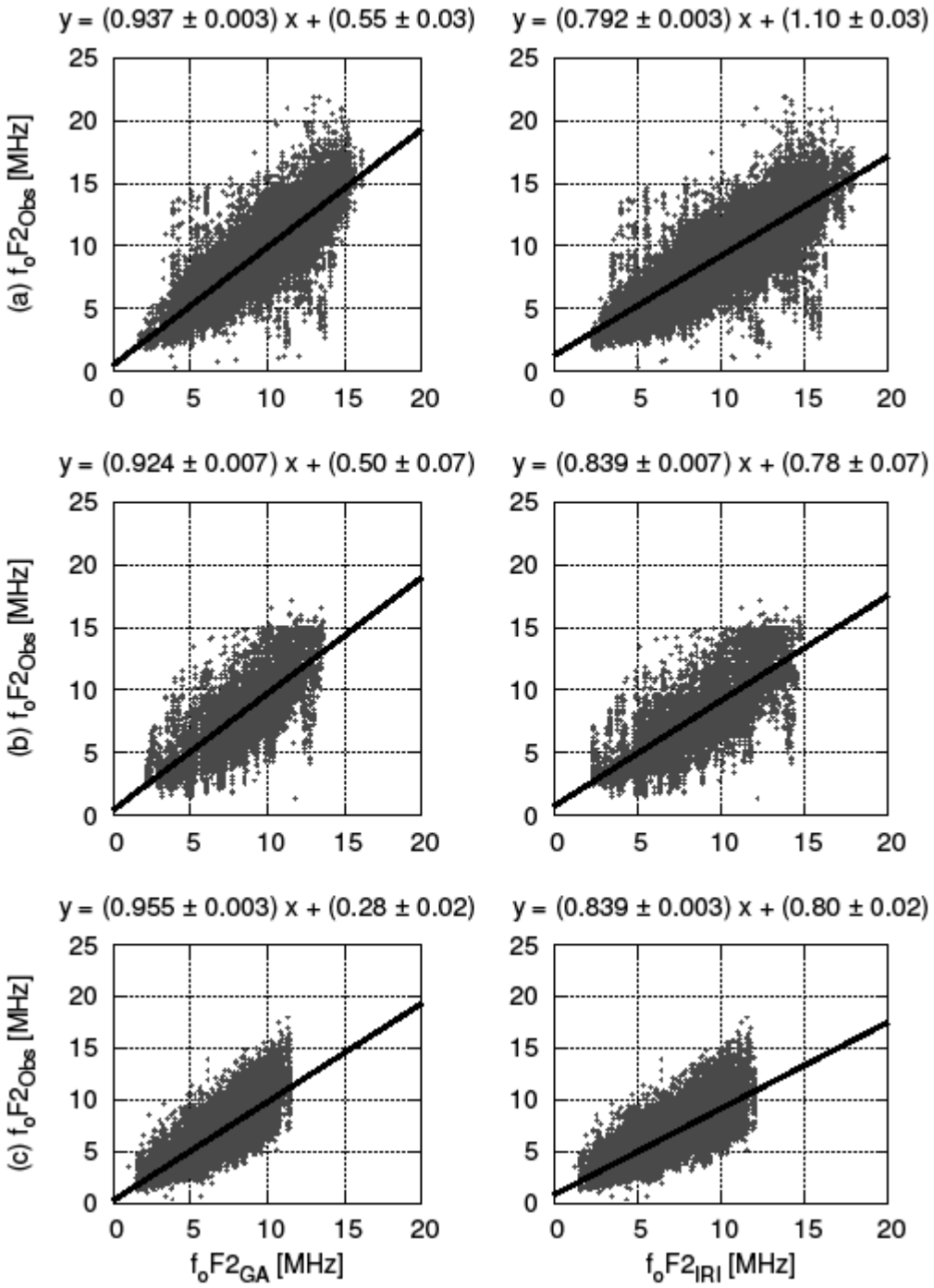

Figure 5. Same as Fig. 3 but for (a) high solar activity, (b) medium solar activity and (c) low solar activity.The straight lines are the least squares fits, whose equations are at the top of each plot.

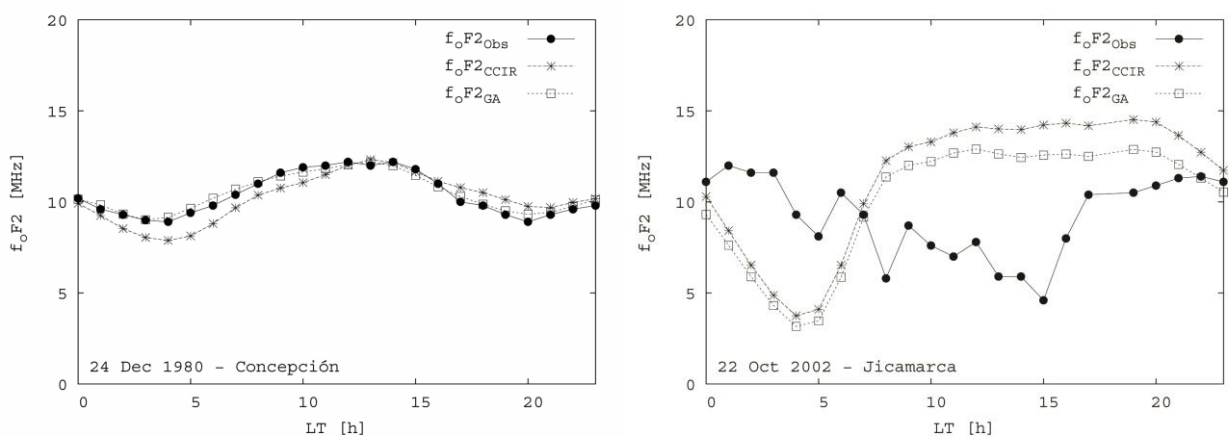

Figure 6. The observed ($f_{\mathrm{o}}F2_{\mathrm{Obs}}$; points), GA-computed ($f_{\mathrm{o}}F2_{\mathrm{GA}}$; squares) and CCIR-computed ($f_{\mathrm{o}}F2_{\mathrm{CCIR}}$; stars) $f_{\mathrm{o}}F2$ values vs. local time (LT) is plotted for: (left) a good and (right) a bad performance day, determined according to the Δf_c quantity (Eq. (7)).

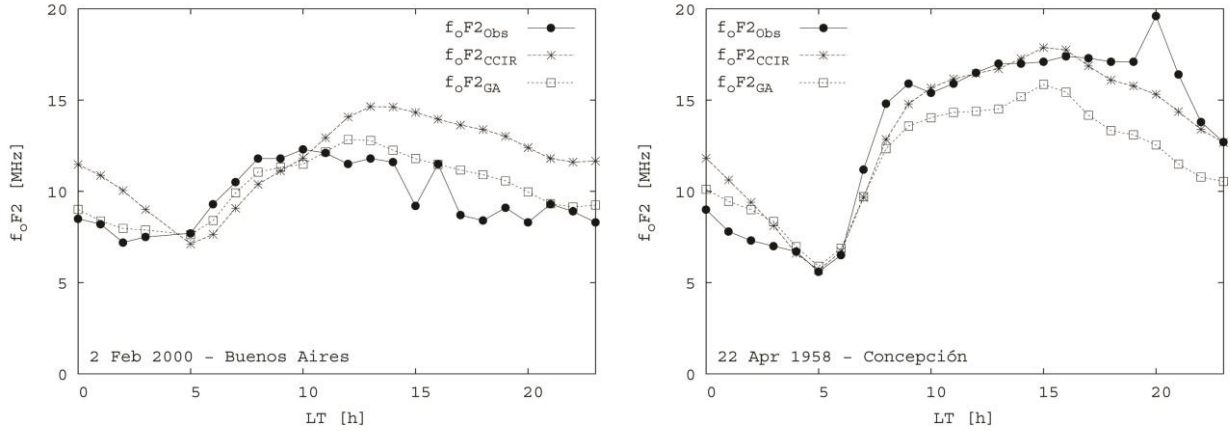

Figure 7. Same as Fig. 6, but the good (left) and bad (right) days determined according to the Δf_{cp} quantity (Eq. (8)).

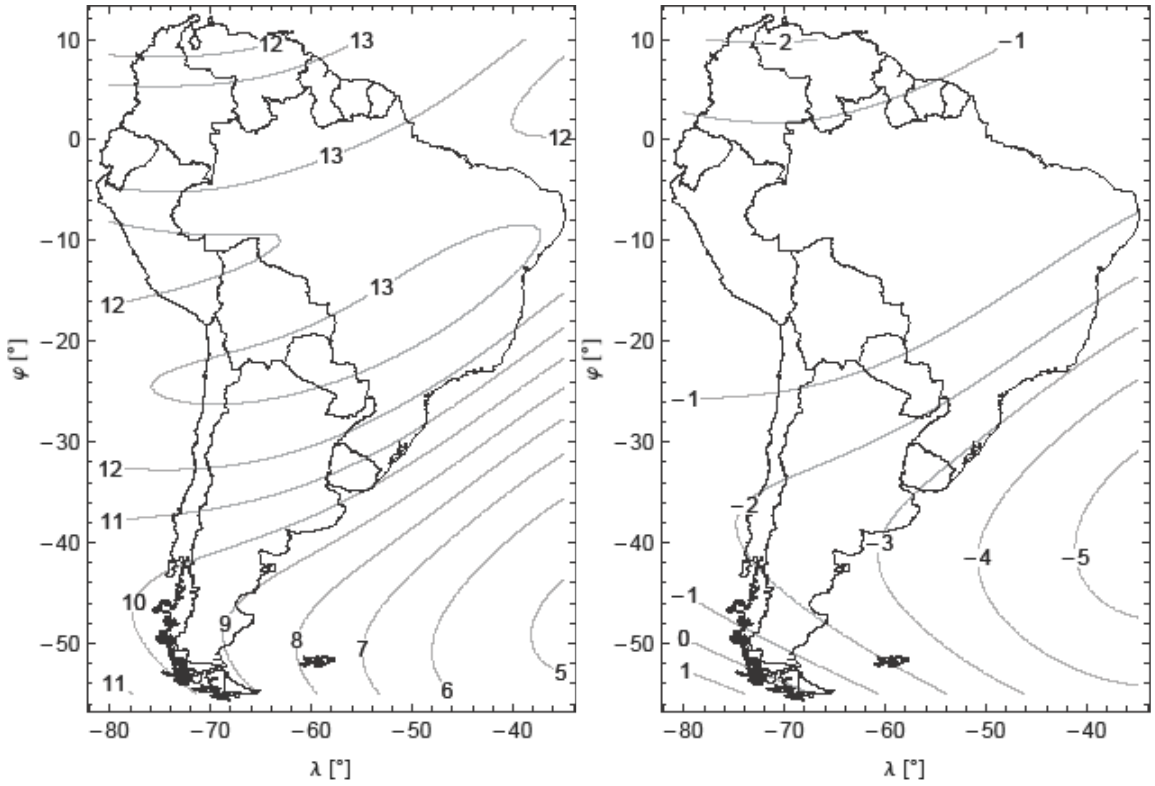

Figure 8. Left: contour map of $f_{\mathrm{o}}F2_{\mathrm{GA}}$ over the South American region at 16:00 local time of the central part, corresponding to February 2nd, 2000. Right: the same, but for the $f_{\mathrm{o}}F2_{\mathrm{GA}} - f_{\mathrm{o}}F2_{\mathrm{CCIR}}$ differences.

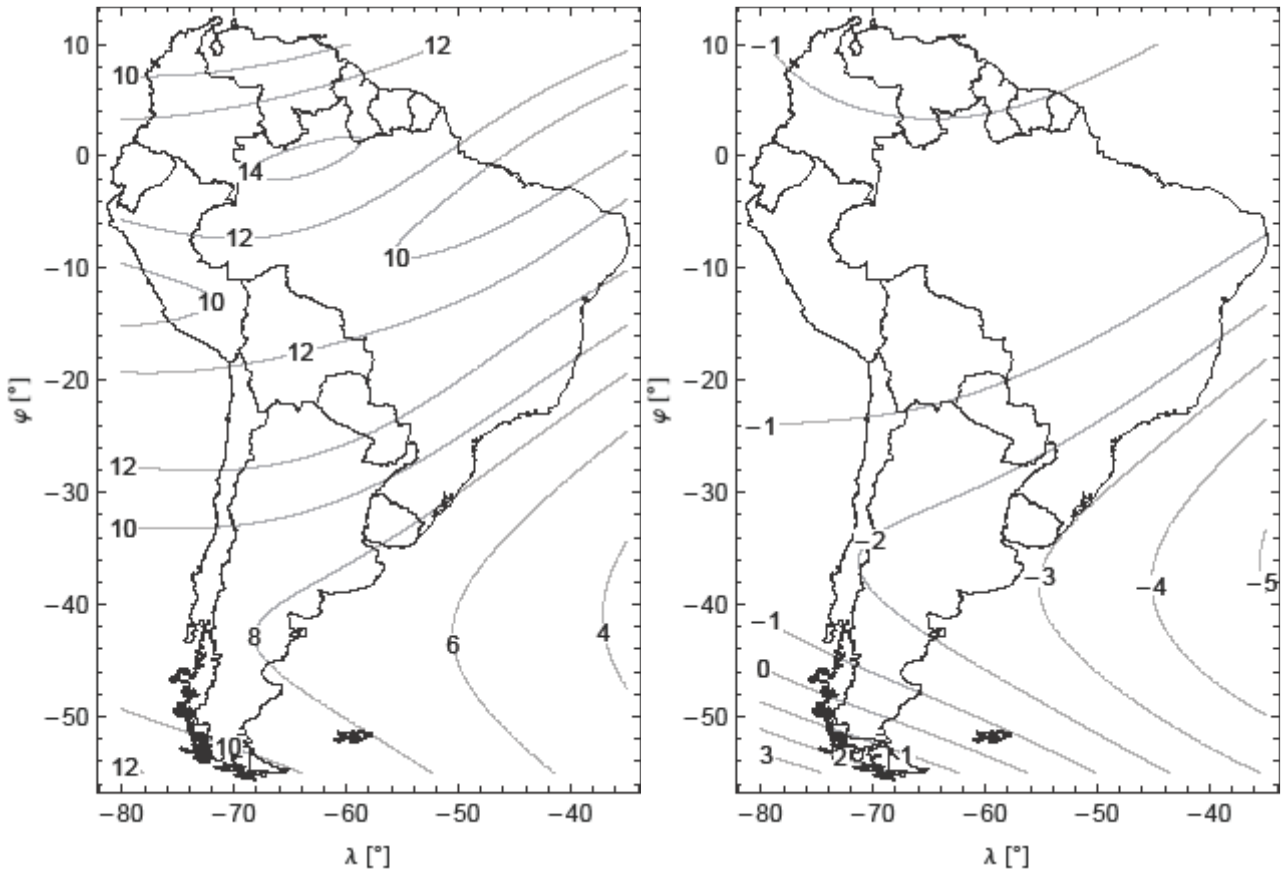

Figure 9. Same as Fig. 8, but at 23:00 local time of the central part.

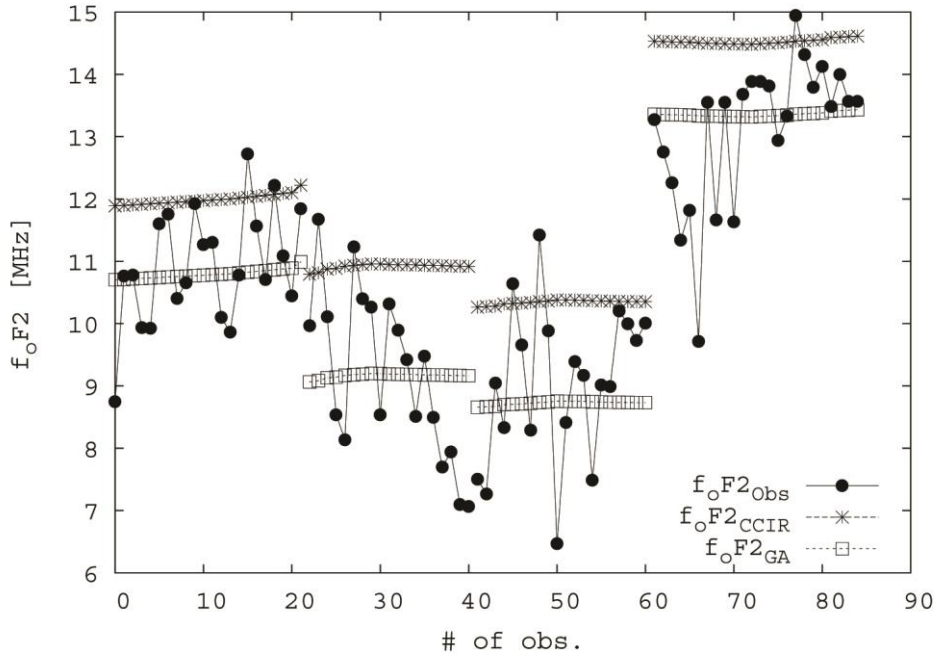

Figure 10. Predictions of the models for the set of observations at La Plata, Argentina. The groups of points from left to right correspond to February, May, August and October of 2012, respectively. All the observations were made at 12:00 local time.

Station	Geographic latitude [°]	Geographic longitude [°]	Modip latitude [°]
Jicamarca	–12.0	283.0	2.73
San Juan	–31.5	290.4	–27.94
Buenos Aires	–34.6	301.7	–31.70
Concepción	–36.8	287.0	–34.44
Trelew	–43.2	294.7	–41.49
Ushuaia	–54.8	291.7	–49.45
San Martín	–68.1	293.0	–60.20

Table 1. Geographic coordinates and modip latitudes of the ionosondes used in this study. Due to their variations along time, modip latitudes are values for reference only.

Parameter		$\rho_{[\mathrm{GA\ Obs}]}$	$\rho_{[\mathrm{CCIR\ Obs}]}$	$\sigma^2_{[\mathrm{GA\ Obs}]}$	$\sigma^2_{[\mathrm{CCIR\ Obs}]}$	$n-1$	*F*
Solar activity	High *IG*12 > 120	0.870	0.823	0.049	0.074	35.621	1.51
	Medium 40 < *IG*12 < 120	0.787	0.767	0.116	0.048	9.449	2.71
	Low *IG*12 < 40	0.860	0.818	0.026	0.036	33.266	1.40
Seasons	Autum	0.898	0.875	0.052	0.079	19.080	1.53
	Spring	0.886	0.856	0.039	0.049	20.441	1.27
	Winter	0.887	0.870	0.053	0.080	19.651	1.50
	Summer	0.855	0.818	0.026	0.032	19.163	1.24
Modip latitude	Equatorial (Jicamarca)	0.509	0.502	0.195	0.275	3.384	1.41
	Low (San Juan)	0.852	0.841	0.079	0.094	9.119	1.19
	Mid (Concepción)	0.943	0.922	0.016	0.029	31.651	1.84
	High (Ushuaia)	0.936	0.900	0.024	0.039	8.406	1.65
	Subauroral (San Martín)	0.886	0.745	0.029	0.040	7.163	1.37
Daily variations	noon [11 h : 14 h]	0.865	0.838	0.054	0.080	13.339	1.53
	midnight [23 h : 2 h]	0.901	0.862	0.036	0.054	12.391	1.56

Table 2. Statistical indicators for the different solar activities, the seasons, the different modip latitudes and the daily variation. The table shows the correlation coefficient $\rho_{[\mathrm{GA\ Obs}]}$ (or $\rho_{[\mathrm{CCIR\ Obs}]}$) between the $f_{\mathrm{o}}F2_{\mathrm{GA}}$ (or $f_{\mathrm{o}}F2_{\mathrm{CCIR}}$) and the $f_{\mathrm{o}}F2_{\mathrm{Obs}}$ values, the dispersion $\sigma^2_{[\mathrm{GA\ Obs}]}$ (or $\sigma^2_{[\mathrm{CCIR\ Obs}]}$), the number of observations (n) and the *F* values (*F*-tests).